Journal of Applied Physics

RESEARCH ARTICLE | JULY 07 2022

Current-induced magnetization switching in epitaxial *L*1$_0$-FePt/Cr heterostructures through orbital Hall effect

H. C. Lyu ; Y. C. Zhao ; J. Qi; G. Yang ; W. D. Qin; B. K. Shao; Y. Zhang; C. Q. Hu; K. Wang; Q. Q. Zhang; J. Y. Zhang ; T. Zhu ; Y. W. Long ; H. X. Wei; B. G. Shen; S. G. Wang

J. Appl. Phys. 132, 013901 (2022)
https://doi.org/10.1063/5.0087562

Journal of Applied Physics ARTICLE scitation.org/journal/jap

Current-induced magnetization switching in epitaxial $L1_0$-FePt/Cr heterostructures through orbital Hall effect

Cite as: J. Appl. Phys. **132**, 013901 (2022); doi: 10.1063/5.0087562
Submitted: 16 May 2022 · Accepted: 18 June 2022 ·
Published Online: 7 July 2022

H. C. Lyu,[1,2] Y. C. Zhao,[2,a)] J. Qi,[1] G. Yang,[3] W. D. Qin,[4] B. K. Shao,[1] Y. Zhang,[1,2] C. Q. Hu,[4] K. Wang,[1] Q. Q. Zhang,[4] J. Y. Zhang,[1] T. Zhu,[2] Y. W. Long,[2] H. X. Wei,[2] B. G. Shen,[2] and S. G. Wang[1,a)]

AFFILIATIONS

[1]Beijing Advanced Innovation Center for Materials Genome Engineering, School of Materials Science and Engineering, University of Science and Technology Beijing, Beijing 100083, China
[2]Beijing National Laboratory for Condensed Matter Physics, Institute of Physics, Chinese Academy of Sciences, Beijing 100190, China
[3]School of Integrated Circuit Science and Engineering, Beihang University, Beijing 100191, China
[4]Institute of Advanced Materials, Beijing Normal University, Beijing 100875, China

[a)]**Authors to whom correspondence should be addressed:** yczhao@iphy.ac.cn and sgwang@ustb.edu.cn

ABSTRACT

The current-induced magnetization switching (CIMS) was successfully observed in epitaxial $L1_0$-FePt/Cr_xPt_{1-x} ($0 \le x \le 1$) heterostructures grown by molecular beam epitaxy with large perpendicular magnetic anisotropy. With increasing Cr content, the critical switching current density (J_c) in FePt/Cr_xPt_{1-x} heterostructures exhibited a decreasing trend, where it was greatly reduced by 69% in FePt/Cr (3*d*) films compared to FePt/Pt (5*d*) films with strong spin–orbit coupling. Furthermore, the same switching polarities were observed for all FePt/Cr_xPt_{1-x} samples, indicating that the orbital Hall effect played a dominant role in CIMS for FePt/Cr films because of opposite spin Hall angles for Cr and Pt. Our results will put forward the applications of $L1_0$-FePt in collaboration with the orbital Hall effect from 3*d* metals in current-controlled magnetic random access memory and neuromorphic computing.

I. INTRODUCTION

Spin–orbit torque (SOT) has been widely investigated for performing efficient manipulation of magnetization in ferromagnet (FM)/non-magnet (NM) heterostructures of various spintronic devices.[1–6] In a traditional scheme, the origin of SOT is usually attributed to the spin Hall effect (SHE) dependent on the strong SOC[7–12] and the Rashba effect due to interfacial symmetry breaking.[13,14] Similar to the SHE, the orbital Hall effect (OHE) generates an orbital current, a flow of orbital angular momentums, which originates from momentum-space orbital textures[15,16] regardless of SOC. Recent reports have pointed out that the non-trivial orbital current can be generated in 3*d* transition metals, graphene, or two-dimensional transition metal dichalcogenides.[17–23] In addition, it has been found that the orbital Hall conductivity (OHC) in 3*d* metals such as V, Cr, Mn, Ni, and Cu is gigantic $\sim 10^3$–10^4 $(\hbar/e)$ $(\Omega\,\mathrm{cm})^{-1}$,[17] which is comparable or even larger than the spin Hall conductivity of Pt.[24–27] However, the orbital current induced by OHE cannot directly provide a torque on magnetization due to the absence of the exchange coupling between orbital angular momentum (L) and local magnetic moment. To motivate the orbit Hall torque (OHT) induced by OHE to exert on the local magnetic moment of the FM, L must be converted to the spin angular momentum (S). Recently, the efficient L–S conversion has been achieved by choosing rare-earth ferromagnetic Gd with strong SOC in Cr/FM structures,[28] which provides an effective pathway to exploit the OHE for the manipulation of the magnetization direction.

Soft magnetic materials, such as Co, Ni, and CoFeB, have been used to investigate the OHE, but the OHE-driven magnetization switching in hard magnetic materials with good perpendicular

magnetic anisotropy (PMA) is very rare. In this Letter, we report a study on $L1_0$-FePt combined with a Cr layer to generate orbital current to switch magnetization, where $L1_0$-FePt has strong SOC as a FM layer together with giant bulk PMA and excellent thermostability and Cr has large orbital Hall conductivity. The current-induced magnetization switching (CIMS) of $L1_0$-FePt with a 3*d* Cr top layer (called Cr-FePt) was successfully achieved through the efficient *L*–*S* conversion. Compared to $L1_0$-FePt with the traditional 5*d* Pt top layer (called Pt-FePt) with strong SOC, the critical switching current density J_c was greatly reduced by 69% in 3*d* Cr-FePt heterostructures, and the feature of the same switching polarity demonstrated the dominating contribution of OHE. Furthermore, the values of J_c for FePt/Cr_xPt_{1-x} films show a decreasing trend with increasing Cr concentration, together with the enhanced switching efficiency. On the other hand, an enhanced spin torque is obtained with increasing Cr thickness, which demonstrates that the orbit current should be generated from the bulk Cr layer, excluding the interfacial orbital Rashba–Edelstein effect (OREE). Remarkably, based on this structure, OHE-induced tunable multistate memristors have been studied, which offers an efficient method of developing $L1_0$-FePt-based neuromorphic computing.

II. EXPERIMENTAL METHOD

The FePt-based heterostructures including FePt(5)/Cr(t)/MgO(2)/Cr(2), FePt (5)/Cr_xPt_{1-x}(10)/MgO(2)/Cr(2) (in nm) were epitaxially deposited on MgO(001) substrates by molecular beam epitaxy (MBE) under a base pressure better than 7×10^{-11} mbar. The deposition of FePt was performed at a relatively low temperature of 300 °C, followed by annealing at a higher temperature of 600 °C to promote the formation of the high-quality $L1_0$ phase. For the deposition of the nonmagnetic layer Cr and Cr_xPt_{1-x}, the temperature was set at 500 °C, followed by 30 min of *in situ* annealing at 600 °C. The prepared films were cooled down to room temperature (RT) before the deposition of 2 nm MgO and 2 nm Cr protection layers. The formation of epitaxial structure and high-quality surface were identified by *in situ* reflection high energy electron diffraction (RHEED) as illustrated in Fig. 1(a).

III. RESULTS AND DISCUSSION

Figures 1(b)–1(d) show the RHEED patterns for MgO substrate, 5 nm FePt ,and 10 nm Cr layers with the e-beam along the MgO[100] direction, respectively. The sharp streaky RHEED patterns indicate high-quality and flat surfaces. Figure 1(e) shows the x-ray diffraction (XRD) measurements of FePt(5)/Cr(10) (in nm) bilayers, where the intense (001) peak indicates the formation of $L1_0$ ordered face-centered-tetragonal (FCT) structure, and (001)-oriented Cr structure is also displayed. Based on the above results, the epitaxial relationship can be determined as MgO(001) [100] || FePt(001) [100] || Cr(001) [110]. Figure 1(f) shows the Hall loops for FePt (5)/Cr(10) (in nm) bilayers with out-of-plane and in-plane magnetic fields applied, exhibiting a strong PMA.

To perform transport measurements, the films were fabricated into Hall bar devices with a width of 10 μm by conventional lithography and ion milling. Then, the CIMSs were performed by applying pulsed current with the width of 1 ms injected along the MgO[110] direction, and the Hall resistance was measured after a 10 s delay under an in-plane field along the applied current directions at RT. The field-dependent CIMSs of Cr-FePt and Pt-FePt heterostructures (here, $t_{FePt} = 5$ nm, $t_{Cr} = t_{Pt} = 10$ nm) were systematically studied for an overall comparison. Figures 2(a) and 2(b) present the CIMS loops of Cr-FePt and Pt-FePt heterostructures under different H_x's, respectively, exhibiting the same switching polarity. Because of opposite spin Hall angles for Cr and Pt,[17,29] this switching feature demonstrates that the OHE of Cr plays a dominating role in the SOT switching of FePt/Cr films, similar to other FM/Cr films.[28] The critical switching current density J_c through the NM layer can be obtained via $J_{c(NM)} = I_{c(total)}/[(1+s)\cdot t_{NM}]$, where s is the shunting parameter, defined as $s = \frac{I_{FM}}{I_{NM}}$. The respective layer resistivities can be obtained from experiments as shown in Table S1 (see the supplementary material), and the corresponding values of s for various Cr contents in FePt/Cr_xPt_{1-x} are 0.34, 0.40, 0.74, 0.71, and 1.61, respectively. The critical switching current density J_c decreases with increasing the amplitude of H_x as summarized in Fig. 2(c), and this feature in Cr-FePt films is more obvious compared to Pt-FePt samples. For Cr-FePt films, H_x not only breaks the switching symmetry of the spin torque, but also significantly reduces the switching energy barrier. In addition, the value of J_c in Cr-FePt films ($\sim 1.1 \times 10^7$ A/cm^2) is reduced by 69% compared to that in Pt-FePt films ($\sim 3.5 \times 10^7$ A/cm^2), which indicates a fascinating performance on SOT switching for Cr-FePt films. For a detailed study, CIMS in FePt/Cr_xPt_{1-x} with varying Cr contents was systematically investigated. Figure 2(d) presents the successive evolution of J_c with different Cr contents in the Cr_xPt_{1-x} layer, indicating a decreasing trend with increasing Cr content. It is worthy to point out that this variation of J_c is not consistent with the nonmonotonic evolution of Cr_xPt_{1-x}(111)/Co/MgO multilayers reported by Hu *et al.*,[30] which is likely related to the strong SOC of the FePt layer and different crystalline orientations. As an FM layer with strong spin–orbit coupling (SOC), FePt is able to fulfill the efficiency of OHE from the Cr layer to achieve a significant *L*–*S* conversion, and NM layer with different crystal orientations will cause different SOT efficiencies.[31–33] Both of these factors contribute to the variation of J_c in FePt/Cr_xPt_{1-x} films. Furthermore, the anisotropy field H_K is measured, which first increases and then decreases with increasing Cr doping content, as shown in Fig. 2(e). The current-induced magnetization switching efficiency, defined as $\eta_{SOT} = H_K/J_c$, was enhanced with increasing Cr doping content as depicted in Fig. 2(f).

To quantitatively investigate the spin-torque efficiency in Cr-FePt films, the harmonic measurements were carried out with external magnetic fields H_x parallel and H_y perpendicular to the current direction as shown in Figs. 3(a) and 3(b), respectively. The first V_ω and second $V_{2\omega}$ harmonic Hall voltage signals of Cr-FePt films were detected simultaneously by two lock-in amplifier systems. Before the harmonic measurements, a large out-of-plane field was applied to saturate the magnetization $\boldsymbol{M}_z$ of the devices, which remains saturated after the field is removed. The selected results of the 10 nm-thick Cr-FePt films by applying a sinusoidal AC with an amplitude of 9 mA were plotted against magnetic fields in Figs. 3(a) and 3(b), in which the signals were measured with the configurations of out-of-plane magnetization component $\boldsymbol{M}_z > 0$ and $\boldsymbol{M}_z < 0$, respectively. The damping-like effective fields H_{DL} and

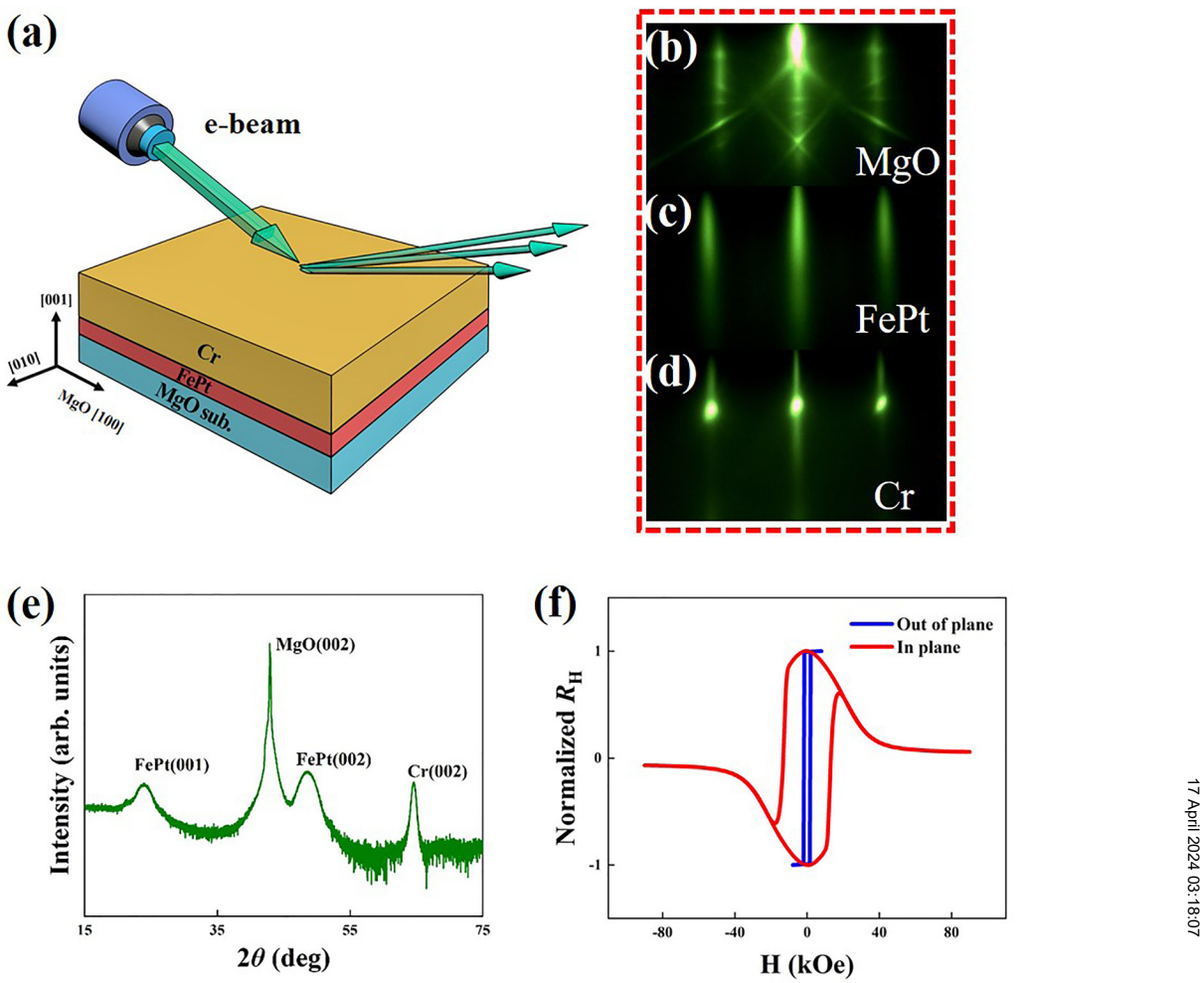

FIG. 1. (a) The schematic RHEED characterization. RHEED patterns with an e-beam along the MgO[100] direction for (b) MgO substrate, (c) FePt layer, and (d) Cr layer, respectively. (e) XRD $\theta - 2\theta$ scan for MgO(001)/FePt(5)/Cr(10) (in nm) films. (f) Hall loops with the sweeping field along the in-plane and out-of-plane directions for MgO (001)/FePt(5)/Cr(10) (in nm) films.

the field-like effective fields H_{FL} can be calculated by the following equation:[34]

$$H_{DL(FL)} = -2\frac{B_{X(Y)} \pm 2\xi B_{Y(X)}}{1-4\xi^2}, \quad (1)$$

where ξ is the ratio of planar Hall effect (PHE) resistance and anomalous Hall effect (AHE) resistance, and the $\pm$ sign corresponds to the magnetization pointing to the $\pm z$ axis. $B_{X(Y)}$ can be determined using the following equation:[5]

$$B_{X(Y)} = \frac{\partial V_{2\omega}}{\partial H_{x(y)}} \Big/ \frac{\partial^2 V_{\omega}}{\partial H_{x(y)}^2}. \quad (2)$$

The value of ξ can be usually neglected on account of its negligible magnitude. According to Eqs. (1) and (2), the calculated H_{DL} and H_{FL} for the FePt/Cr_xPt_{1-x} films with various Cr concentrations are shown in Fig. 3(c). It is obvious that the value of H_{DL} and H_{FL} decreases with increasing Cr content. It should be noted that the magnitudes of H_{FL} are much smaller for all samples compared to H_{DL}, suggesting the dominating contributions from damping-like torques in FePt/NM configurations.

In the simplified models in the macrospin limit[35] [Eq. (3)] and in the domain-wall depinning regime[36] [Eq. (4)], J_c can be expressed as

$$J_c = \frac{e\mu_0 M_s t_{FM}\left(H_K - \sqrt{2}|H_x|\right)}{\hbar\xi_{DL}}, \quad (3)$$

$$J_c = \frac{4e\mu_0 M_s t_{FM} H_c}{\pi\hbar\xi_{DL}}, \quad (4)$$

where M_s is the saturation magnetization, ξ_{DL} is the damping-like SOT efficiency of the system, H_K is the effective perpendicular anisotropy field, and H_c is the perpendicular coercivity of the FM, respectively. According to the above models, the ratio of anisotropy field to spin-torque efficiency H_K/β_{DL} in Eq. (3) was calculated, together with the ratio of coercivity field to spin-torque efficiency H_c/β_{DL} in Eq. (4) as portrayed in Fig. 3(d). H_K/β_{DL} increases sharply with increasing Cr content, which means that a larger J_c is

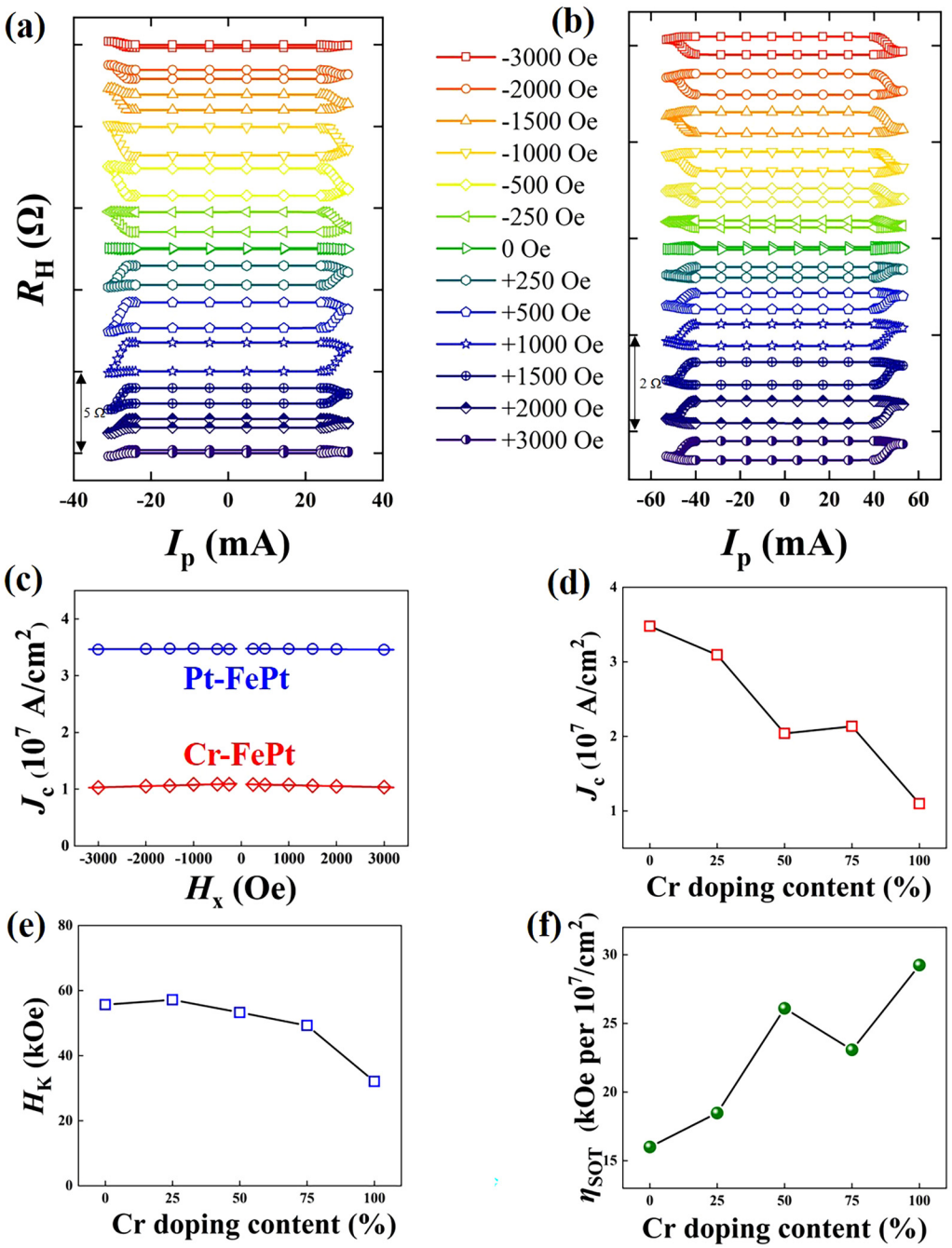

FIG. 2. SOT switching loops obtained under varying H_x for (a) Cr-FePt and (b) Pt-FePt films. (c) J_c as a function of H_x for Cr-FePt and Pt-FePt films. (d) Cr doping content dependence of J_c. (e) The anisotropy field H_K and (f) switching efficiency η_{SOT} as a function of Cr doping content.

required for the magnetization switching in Cr-FePt films. This is contrary to the experimental findings. Moreover, the nonmonotonic variation of H_c/β_{DL} cannot explain the reduction of J_c either. Therefore, the reduced J_c cannot be reasonably interpreted only by these terms, and more effects should be taken into account for SOT-driven magnetization switching.

The aforementioned simplified models are obtained in the absence of the field-like torque. However, when the field-like torque is included, the threshold switching current would be dependent on the damping constant.[37] In addition, the relation between the threshold switching current and damping parameter dependent on the ratio of H_{FL} to H_{DL} η was further discussed theoretically.[38] Hence, the contribution from damping likely needs to be considered if there is a significant field-like torque in the perpendicular magnetized systems. In this work, considering that the field-like torque in FePt/Pt films is very large (approximately 41.0 Oe per 10^7 A/cm^2), the large damping of FePt (the value of 0.2 reported by He *at al.*[39]) may increase the difficulty of switching. With increasing Cr doping content, the field-like toque and damping constant in the film system are both reduced (the evidence of the reduced damping constant was reported by Hu *et al.*[30]), the weight of the damping would go down, thereby reducing the threshold current density.

Figure 4(a) illustrates the conversion process in the FePt/Cr heterostructure, where L_{OHE} originating from Cr is converted to S_{OHE} in the FePt layer. Since FePt has a positive η_{L-S}^{FePt} because of its positive spin Hall angle,[40] S_{OHE} would be positive ($\sigma_{OH}^{Cr}\eta_{L-S}^{FePt} > 0$), while S_{SHE} is negative ($\sigma_{SH}^{Cr} < 0$). Thus, the OHT due to S_{OHE} is

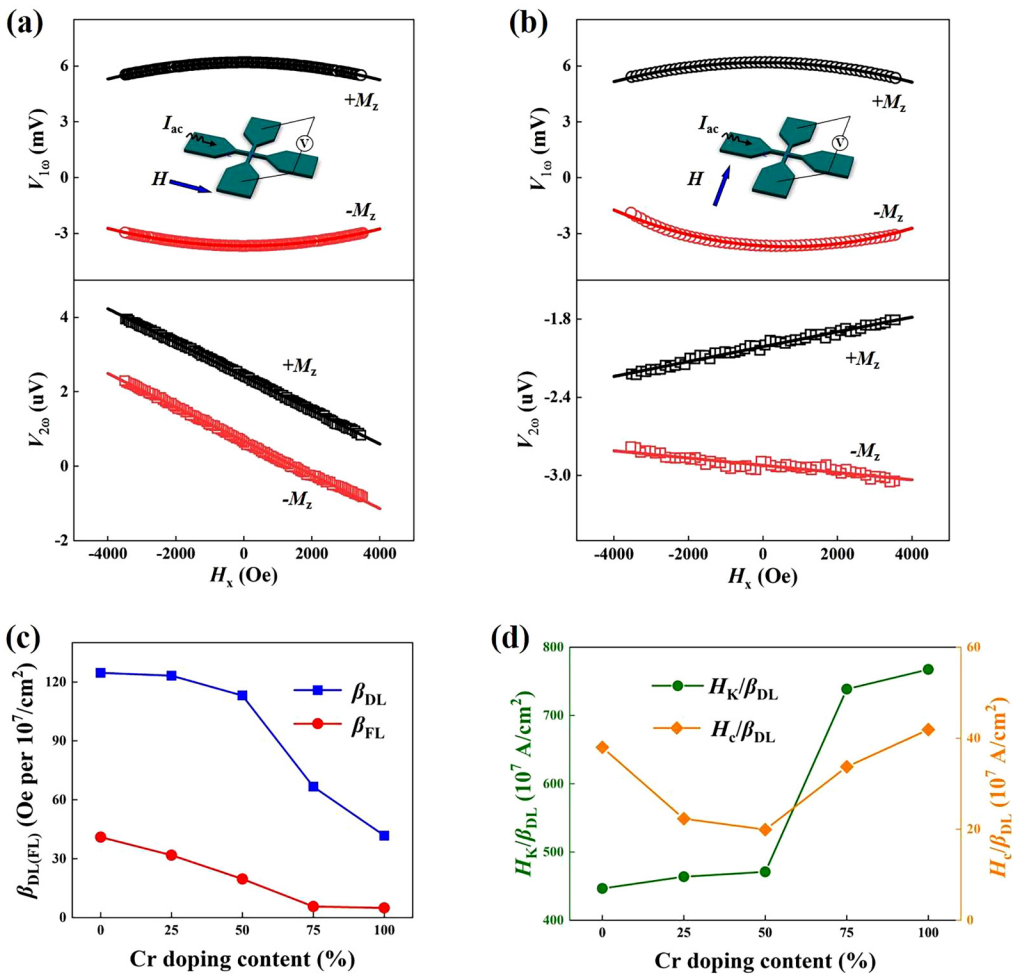

FIG. 3. (a) The first and second harmonic signals in the fully saturated magnetic states (magnetic states pointing near +z or −z are indicated by $+M_z$ and $-M_z$, respectively) with an in-plane magnetic field along (a) and transverse (b) to the current direction. (c) The derived effective fields as a function of Cr doping content. (d) H_K/β_{DL} (green line) and H_c/β_{DL} (orange line) as a function of Cr doping content.

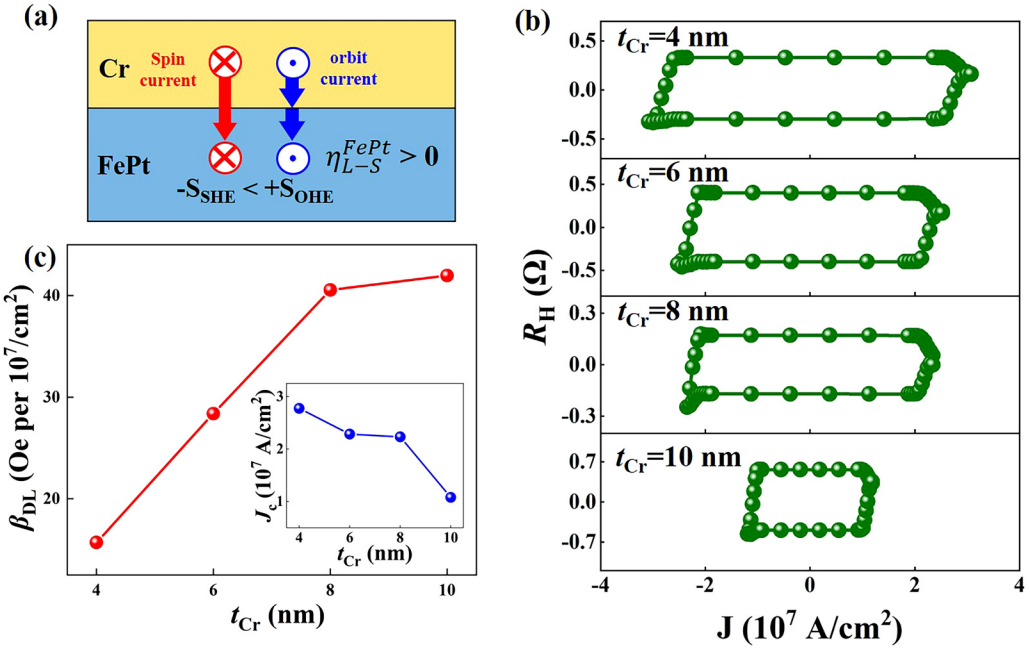

FIG. 4. (a) Schematic illustrations of the angular momentum transfer by spin current (red arrows) and orbital current (blue arrows) for the FePt film with a strong SOC. The spin (orbital) angular momentum is represented by *S* (*L*). (b) CIMS under +1000 Oe magnetic field for different values of t_{Cr}. (c) The SOT efficiency as a function of t_{Cr}. The inset shows t_{Cr} dependence of J_c.

the opposite of the spin Hall torque (SHT) due to S_{SHE}. According to the recent report, the interfacial OREE may also be an important resource for the generation of the orbit current.[23,41] To rule out this possibility, the CIMS with various t_{Cr} for the samples was investigated as shown in Fig. 4(b), where t_{Cr} ranges from 4 to 10 nm. It is found that J_c decreases monotonically with increasing t_{Cr}. Furthermore, the magnitude of damping-like torque efficiency increases with increasing t_{Cr} after considering the shunting effect of metallic layers as shown in Fig. 4(c), indicating that θ_{SH}^{eff} of Cr-FePt samples predominantly originates from the Cr layer, not from the FePt/Cr interface, and the OHE in Cr is the main source of θ_{SH}^{eff} for the FePt/Cr films. It is worth noting that the potential contribution of the self-torque from the FePt layer is not disentangled from spin torques by the present measurements, but is also not expected to be dominating considering the measured magnitudes of the torques from the FePt single layer and the thickness dependence. For example, the CIMS of the 5 nm FePt single layer was obtained by applying a magnetic field of +500 Oe along the current direction as shown in Fig. S4 in the supplementary material, suggesting an opposite switching polarity compared to the FePt/Cr_xPt_{1-x} films. This indicates that the self-torque from the FePt layer will impede the CIMS performed in FePt/Cr_xPt_{1-x} films. Besides, the measured torque efficiency in the FePt single layer is 7.7 Oe per 10^7 A/cm^2, which is significantly smaller than the measured value for the FePt/Cr_xPt_{1-x} films (41.8–124.6 Oe per 10^7 A/cm^2). And, it has been reported that the spin torques induced by FePt are proportional to the composition gradient and the order degree.[42–44] The contribution of spin torques from the FePt layer in our experiments is relatively little, because only a small composition gradient and low ordering exists due to the selected 5 nm thickness and the deposition temperature of 300 °C for FePt. Therefore, the torques from the NM layer dominate the CIMS of FePt/Cr_xPt_{1-x} films.

The binary states in FePt/Cr heterostructures can be tuned by OHT as discussed above; however, the multilevel storage performance attracts extensive attention with the development of neuromorphic computing, since they can be used to simulate the synapse-like function. Figure 5(a) shows a simple neuromorphic network, where synapses connect neurons. Information spreads by the weight of synapses in the network, and the nonvolatile weight can be enhanced or inhibited by positive or negative stimulation. Under $H_x = +1000$ Oe, a train of positive and negative current pulses with 27 mA are alternately applied as depicted in Fig. 5(b). Correspondingly, the evolution of a stable multilevel remanent Hall resistance has been observed in Fig 5(c). It can be found that with the increasing number of positive (negative) current pulses, R_H gradually increases (decreases) and tends to saturate, which suggests an application-oriented memristive behavior with good stability. The multilevel-stable remanence states driven by OHE in Cr-FePt films show potential applications in future multilevel memories and neuromorphic computing devices.

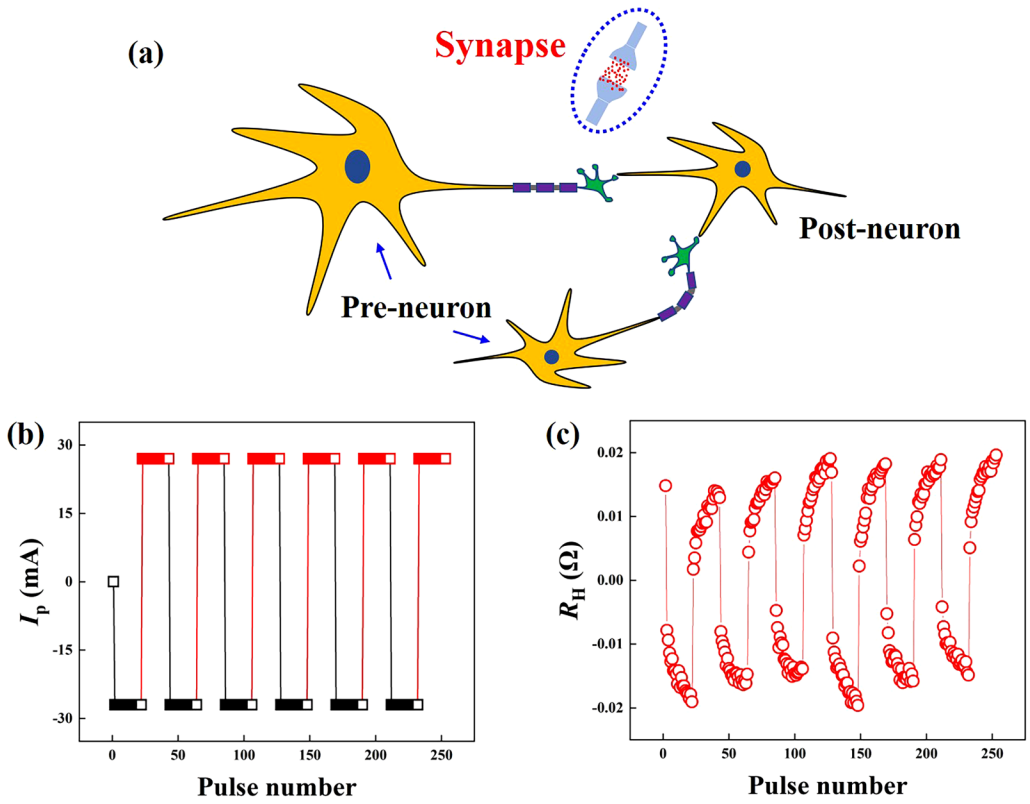

FIG. 5. (a) Schematic drawing of a simple biological synapse network. (b) The applied trains of current pulses with H_x = 1000 Oe, where 21 positive or negative pulses with 27 mA are alternately applied. (c) The response of R_H obtained after (b).

IV. CONCLUSION

In summary, the deterministic CIMS of $L1_0$-FePt can be realized through the non-trivial OHE, originating from the orbital current in the adjacent 3*d* Cr layer. Compared to the traditional 5*d* Pt with strong SOC, the critical switching current density J_c was reduced by 69% in 3*d* Cr-FePt heterostructures. On the other hand, an enhanced SOT efficiency is obtained with increasing t_{Cr}, which demonstrates that the orbital current is generated from the Cr layer instead of the interface. Furthermore, the memristive switching behavior driven by OHE was realized, which shows great potential in low-power performance. These results shed light on CIMS in $L1_0$-FePt/Cr heterostructures and uncover the significant role of 3*d* materials with a variety of functions for next generation spintronic devices.

SUPPLEMENTARY MATERIAL

See the supplementary material for the Cr content-dependent RHEED characterization, anomalous Hall effect, and harmonic Hall measurement.

ACKNOWLEDGMENTS

This work was supported by the National Key Research and Development Program of China (Grant No. 2019YFB2005800), the Science Center of the National Science Foundation of China (Grant No. 52088101), the Natural Science Foundation of China (NSF) (Grant Nos. 52130103, 12174426, 12104486, 51971026, and 11874082), the ISF-NSFC Joint Research Program (Grant No. 51961145305), the State Key Laboratory for Advanced Metals and Materials (Grant No. 2019Z-10), the Beijing Natural Science Foundation Key Program (Grant No. Z190007), and the Fundamental Research Funds for the Central Universities (Grant No. FRF-TP-16-001C2).

AUTHOR DECLARATIONS

Conflict of Interest

The authors have no conflicts to disclose.

Author Contributions

H. C. Lyu: Investigation (equal); Writing – original draft (equal). **Y. C. Zhao:** Writing – review & editing (equal). **J. Qi:** Data curation (equal). **G. Yang:** Formal analysis (equal). **W. D. Qin:** Data curation (equal). **B. K. Shao:** Data curation (equal). **Y. Zhang:** Data curation (supporting). **C. Q. Hu:** Data curation (equal). **K. Wang:** Data curation (equal). **Q. Q. Zhang:** Data curation (equal). **J. Y. Zhang:** Formal analysis (supporting). **T. Zhu:**

Resources (equal). **Y. W. Long:** Resources (equal). **H. X. Wei:** Resources (equal). **B. G. Shen:** Funding acquisition (equal). **S. G. Wang:** Funding acquisition (lead); Supervision (lead).

DATA AVAILABILITY

The data that support the findings of this study are available from the corresponding authors upon reasonable request.

REFERENCES

[1]I. M. Miron, G. Gaudin, S. Auffret, B. Rodmacq, A. Schuhl, S. Pizzini, J. Vogel, and P. Gambardella, Nat. Mater. **9**, 230 (2010).
[2]I. M. Miron, K. Garello, G. Gaudin, P. J. Zermatten, M. V. Costache, S. Auffret, S. Bandiera, B. Rodmacq, A. Schuhl, and P. Gambardella, Nature **476**, 189 (2011).
[3]L. Liu, O. J. Lee, T. J. Gudmundsen, D. C. Ralph, and R. A. Buhrman, Phys. Rev. Lett. **109**, 096602 (2012).
[4]L. Liu, C. F. Pai, Y. Li, H. W. Tseng, D. C. Ralph, and R. A. Buhrman, Science **336**, 555 (2012).
[5]J. Kim, J. Sinha, M. Hayashi, M. Yamanouchi, S. Fukami, T. Suzuki, S. Mitani, and H. Ohno, Nat. Mater. **12**, 240 (2013).
[6]X. Fan, J. Wu, Y. Chen, M. J. Jerry, H. Zhang, and J. Q. Xiao, Nat. Commun. **4**, 1799 (2013).
[7]T. Tanaka, H. Kontani, M. Naito, T. Naito, D. S. Hirashima, K. Yamada, and J. Inoue, Phys. Rev. B **77**, 165117 (2008).
[8]Y. Sun, Y. Zhang, C. Felser, and B. Yan, Phys. Rev. Lett. **117**, 146403 (2016).
[9]D. Sun, K. J. van Schooten, M. Kavand, H. Malissa, C. Zhang, M. Groesbeck, C. Boehme, and Z. Valy Vardeny, Nat. Mater. **15**, 863 (2016).
[10]L. Zhu and R. A. Buhrman, Phys. Rev. Appl. **12**, 051002 (2019).
[11]J. Sinova, S. O. Valenzuela, J. Wunderlich, C. H. Back, and T. Jungwirth, Rev. Mod. Phys. **87**, 1213 (2015).
[12]J. Y. Zhang, P. W. Dou, W. L. Peng, J. Qi, J. Q. Liu, R. Y. Liu, X. Q. Zheng, Y. F. Wu, H. C. Lyu, Y. C. Zhao, Z. Z. Zhu, C. Y. You, A. Kohn, and S. G. Wang, Appl. Phys. Lett. **117**, 232406 (2020).
[13]H. C. Koo, S. B. Kim, H. Kim, T. E. Park, J. W. Choi, K. W. Kim, G. Go, J. H. Oh, D. K. Lee, E. S. Park, I. S. Hong, and K. J. Lee, Adv. Mater. **32**, 2002117 (2020).
[14]D. Di Sante, P. Barone, R. Bertacco, and S. Picozzi, Adv. Mater. **25**, 509 (2013).
[15]D. Go, D. Jo, C. Kim, and H. W. Lee, Phys. Rev. Lett. **121**, 086602 (2018).
[16]D. Go and H.-W. Lee, Phys. Rev. Res. **2**, 013177 (2020).
[17]D. Jo, D. Go, and H.-W. Lee, Phys. Rev. B **98**, 214405 (2018).
[18]S. Bhowal and S. Satpathy, Phys. Rev. B **101**, 121112(R) (2020).
[19]L. M. Canonico, T. P. Cysne, A. Molina-Sanchez, R. B. Muniz, and T. G. Rappoport, Phys. Rev. B **101**, 161409(R) (2020).
[20]S. Bhowal and S. Satpathy, Phys. Rev. B **102**, 035409 (2020).
[21]S. Bhowal and G. Vignale, Phys. Rev. B **103**, 195309 (2021).
[22]T. P. Cysne, M. Costa, L. M. Canonico, M. B. Nardelli, R. B. Muniz, and T. G. Rappoport, Phys. Rev. Lett. **126**, 056601 (2021).
[23]Z. C. Zheng, Q. X. Guo, D. Jo, D. Go, L. H. Wang, H. C. Chen, W. Yin, X. M. Wang, G. H. Yu, W. He, H. W. Lee, J. Teng, and T. Zhu, Phys. Rev. Res. **2**, 013127 (2020).
[24]Q. N. Bai, Y. B. Zhai, J. J. Yun, J. R. Zhang, M. X. Chang, Y. L. Zuo, and L. Xi, Appl. Phys. Lett. **119**, 212404 (2021).
[25]Y. Wang, P. Deorani, X. Qiu, J. H. Kwon, and H. Yang, Appl. Phys. Lett. **105**, 152412 (2014).
[26]Y. Deng, M. Yang, Y. Ji, and K. Wang, J. Magn. Magn. Mater. **496**, 165920 (2020).
[27]Y. Sheng, Y. C. Li, X. Q. Ma, and K. Y. Wang, Appl. Phys. Lett. **113**, 112406 (2018).
[28]S. Lee, M.-G. Kang, D. Go, D. Kim, J.-H. Kang, T. Lee, G.-H. Lee, J. Kang, N. J. Lee, Y. Mokrousov, S. Kim, K.-J. Kim, K.-J. Lee, and B.-G. Park, Commun. Phys. **4**, 234 (2021).
[29]D. Qu, S. Y. Huang, and C. L. Chien, Phys. Rev. B **92**, 020418(R) (2015).
[30]C.-Y. Hu, Y.-F. Chiu, C.-C. Tsai, C.-C. Huang, K.-H. Chen, C.-W. Peng, C.-M. Lee, M.-Y. Song, Y.-L. Huang, S.-J. Lin, and C.-F. Pai, ACS Appl. Electron. Mater. **4**, 1099 (2022).
[31]J. Ryu, C. O. Avci, S. Karube, M. Kohda, G. S. D. Beach, and J. Nitta, Appl. Phys. Lett. **114**, 142402 (2019).
[32]X. F. Zhou, J. Zhang, F. Li, X. Z. Chen, G. Y. Shi, Y. Z. Tan, Y. D. Gu, M. S. Saleem, H. Q. Wu, and F. Pan, Phys. Rev. Appl. **9**, 054028 (2018).
[33]W. Zhang, W. Han, S.-H. Yang, Y. Sun, Y. Zhang, B. Yan, and S. S. P. Parkin, Sci. Adv. **2**, 1600759 (2016).
[34]M. Hayashi, J. Kim, M. Yamanouchi, and H. Ohno, Phys. Rev. B **89**, 144425 (2014).
[35]K.-S. Lee, S.-W. Lee, B.-C. Min, and K.-J. Lee, Appl. Phys. Lett. **102**, 112410 (2013).
[36]T.-Y. Chen, C.-T. Wu, H.-W. Yen, and C.-F. Pai, Phys. Rev. B **96**, 104434 (2017).
[37]T. Taniguchi, S. Mitani, and M. Hayashi, Phys. Rev. B **92**, 024428 (2015).
[38]D. Zhu and W. Zhao, Phys. Rev. Appl. **13**, 044078 (2020).
[39]P. He, X. Ma, J. W. Zhang, H. B. Zhao, G. Lüpke, Z. Shi, and S. M. Zhou, Phys. Rev. Lett. **110**, 077203 (2013).
[40]T. Seki, S. Iihama, T. Taniguchi, and K. Takanashi, Phys. Rev. B **100**, 144427 (2019).
[41]S. Ding, A. Ross, D. Go, L. Baldrati, Z. Ren, F. Freimuth, S. Becker, F. Kammerbauer, J. Yang, G. Jakob, Y. Mokrousov, and M. Kläui, Phys. Rev. Lett. **125**, 177201 (2020).
[42]M. Tang, K. Shen, S. Xu, H. Yang, S. Hu, W. Lü, C. Li, M. Li, Z. Yuan, S. J. Pennycook, K. Xia, A. Manchon, S. Zhou, and X. Qiu, Adv. Mater. **32**, 2002607 (2020).
[43]S. Q. Zheng, K. K. Meng, Q. B. Liu, J. K. Chen, J. Miao, X. G. Xu, and Y. Jiang, Appl. Phys. Lett. **117**, 242403 (2020).
[44]L. Liu, J. Yu, R. González-Hernández, C. Li, J. Deng, W. Lin, C. Zhou, T. Zhou, J. Zhou, H. Wang, R. Guo, H. Y. Yoong, G. M. Chow, X. Han, B. Dupé, J. Železný, J. Sinova, and J. Chen, Phys. Rev. B **101**, 220402(R) (2020).